Photo-induced double-strand DNA and site-specific protein cleavage activity of L-histidine (μ-oxo)diiron(III) complexes of heterocyclic bases†

Mithun Roy,[a] Tuhin Bhowmick,[b] Ramkumar Santhanagopal,[a] Suryanarayana Ramakumar[b] and Akhil R. Chakravarty*[a]

Received 21st January 2009, Accepted 26th March 2009
First published as an Advance Article on the web 27th April 2009
DOI: 10.1039/b901337g

Three oxo-bridged diiron(III) complexes of L-histidine and heterocyclic bases $[Fe_2(\mu\text{-}O)(L\text{-}his)_2(B)_2](ClO_4)_2$ (**1–3**), where B is 2,2′-bipyridine (bpy), 1,10-phenanthroline (phen), dipyrido[3,2-*d*:2′,3′-*f*]-quinoxaline (dpq), were prepared and characterized. The bpy complex **1** was structurally characterized by X-ray crystallography. The molecular structure showed a $\{Fe_2(\mu\text{-}O)\}$ core in which iron(III) in a FeN_4O_2 coordination is bound to tridentate monoanionic L-histidine and bidentate bpy ligands. The Fe···Fe distance is ~3.5 Å. The Fe–O–Fe unit is essentially linear, giving a bond angle of ~172°. The complexes showed irreversible cyclic voltammetric cathodic response near –0.1 V *vs.* SCE in H_2O–0.1 M KCl. The binuclear units displayed antiferromagnetic interaction between two high-spin ($S = 5/2$) iron(III) centers giving a $-J$ value of ~110 cm^{-1}. The complexes showed good DNA binding propensity giving a binding constant value of ~10^5 M^{-1}. Isothermal titration calorimetric data indicated single binding mode to the DNA. The binding was found to be driven by negative free energy change and enthalpy. The dpq complex **3** showed oxidative double-strand DNA cleavage on exposure to UV-A and visible light. The phen complex **2** displayed single-strand photocleavage of DNA. The DNA double-strand breaks were rationalized from theoretical molecular docking calculations. Mechanistic investigations showed formation of hydroxyl radicals as the reactive species through photodecarboxylation of the L-histidine ligand. The complexes exhibited good binding propensity to bovine serum albumin (BSA) protein in Tris-HCl/NaCl buffer medium. The dpq complex **3** showed UV-A light-induced site-specific oxidative BSA cleavage forming fragments of ~45 kDa and ~20 kDa molecular weights *via* $^{\bullet}OH$ pathway.

Introduction

Metal-based synthetic nucleases and proteases are of importance for their various applications in nucleic acid and peptide chemistry, *viz.* as restriction enzyme mimics, foot-printing agents, model peptidases and as therapeutic agents.[1–10] Oxidative cleavage of DNA by model nucleases involves the deoxyribose moiety or guanine base in phototherapeutic applications like photodynamic therapy (PDT) of cancer.[11–15] PDT is a non-invasive treatment modality in which the cancer cells are selectively targeted by red light of 600–800 nm wavelength thus damaging only the cancer cells leaving the healthy cells unaffected. Porphyrin and phthalocyanin bases have been studied as PDT agents.[11] The PDT drug Photofrin® is the mixture of hematoporphyrin species. Porphyrin bases are known to be hepatotoxic due to bilirubin formation on oxidative conversion.[16] This has generated current interests to develop the chemistry of metal-based PDT agents.

While a variety of organic dyes have been used as potent PDT agents, the chemistry of metal-based complexes remains largely unexplored.[17–25] The present work stems from our interest in developing the chemistry of 3d metal complexes as photocleavers of DNA within the PDT spectral window.[26–30] Our recent reports have shown that ternary iron(III) complexes having photoactive dipyrido[3,2-*d*:2′,3′-*f*]quinoxaline (dpq) or dipyrido[3,2-*a*:2′,3′-*c*]phenazine (dppz) ligand cleave DNA efficiently on photoirradiation of the metal-centered charge transfer band in visible light.[31,32] We have also reported a (μ-oxo)diiron(III) complex $[\{Fe(L\text{-}his)(dpq)\}_2(\mu\text{-}O)]^{2+}$ of L-histidine (L-his) and dpq showing DNA double-strand breaks on exposure to visible light.[33] Double-strand DNA cleavage is of importance in terms of greater cell lethality than the single-strand cleavage. The natural antitumor antibiotic iron-bleomycins (Fe-BLMs) are known to show double-strand DNA cleavage.[34] Synthetic models of Fe-BLMs showing such activity are, however, rare and are limited to complexes acting as "chemical nucleases" in the presence of external additives.[35,36]

Synthetic proteases that can cleave protein backbone with a high specificity are useful as multifunctional biochemical agents suitable for understanding the structure–activity correlations of proteins and towards exploring different structural domains in proteins.[37–42] Like model photonucleases, synthetic photoproteases that degrade protein under physiological conditions are of interest for selectively controlling specific protein functions.[43–47] Kumar and coworkers have reported cobalt-based model photoproteases

[a]*Department of Inorganic and Physical Chemistry, Indian Institute of Science, Bangalore, 560012, India. E-mail: arc@ipc.iisc.ernet.in; Fax: +91-80-23600683; Tel: +91-80-22932533*
[b]*Bioinformatics Centre, Department of Physics, Indian Institute of Science, Bangalore, 560012, India*

† Electronic supplementary information (ESI) available: Figures on spectral, magnetic, redox, DNA and protein binding and cleavage (Fig. S1–S14). CCDC reference number 678207. For ESI and crystallographic data in CIF or other electronic format see DOI: 10.1039/b901337g

that are effective in inducing site-specific cleavage of bovine serum albumin (BSA) and lysozyme proteins on exposure to UV-A light.[48–50] Synthetic proteases are also of importance in the emerging chemistry of anti-metastasis agents to control tumor malignancy.[51–54] Herein, we report three oxo-bridged diiron(III) complexes $[\{Fe(L\text{-his})(B)\}_2(\mu\text{-}O)](ClO_4)_2$ (**1–3**) of L-histidine and heterocyclic bases as model metal-based photonucleases and photoproteases, where B is 2,2′-bipyridine (bpy) in **1**; 1,10-phenanthroline (phen) in **2**; and dpq in **3** (Fig. 1). A preliminary report of this work has been made.[33]

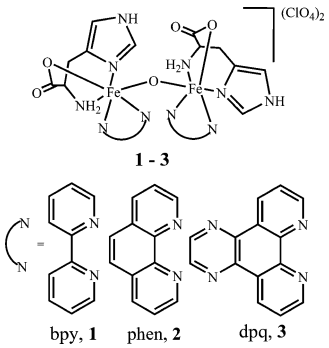

Fig. 1 The complexes **1–3** and the heterocyclic bases used.

Experimental

Materials and measurements

The reagents and chemicals were obtained from commercial sources and used as received without any further purification. The solvents used were purified by standard methods.[55] The supercoiled (SC) pUC19 DNA (cesium chloride purified) was purchased from Bangalore Genie (India). Calf thymus (CT) DNA, agarose (molecular biology grade), distamycin-A, catalase, SOD and ethidium bromide (EB), 2,2,6,6-tetramethyl-4-piperidone (TEMP), bovine serum albumin (BSA), acrylamide, *N*,*N*′-methylenebisacrylamide, ammonium persulfate, *N*,*N*,*N*′,*N*′-tetramethylethylene-diamine (TEMED), 2-mercaptoethanol (MPE), glycerol, sodium dodecyl sulfate (SDS), bromophenol blue, coomassie brilliant blue R-250 were from Sigma (USA). Tris(hydroxymethyl)aminomethane–HCl (Tris–HCl) buffer was prepared using deionized and sonicated triple distilled water. Dipyrido[3,2-*d*:2′,3′-*f*]quinoxaline was synthesized according to the literature procedure.[56]

The elemental analysis was performed using a Thermo Finnigan FLASH EA 1112 CHNS analyzer. The infrared and electronic spectra were recorded on PerkinElmer Lambda 35 and PerkinElmer spectrum one 55 spectrophotometers, respectively. Electrospray ionization mass, MALDI TOF MS and EPR spectral measurements were done using Bruker Daltonics make Esquire 300 Plus ESI Model, Bruker Daltonics made Ultraflex MALDI TOF/TOF mass spectrometer and Bruker EMX spectrometer, respectively. Variable temperature magnetic susceptibility data in the range of 300–20 K for powdered samples of the complexes were obtained using Model 300 Lewis-coil-force magnetometer of George Associates Inc. (Berkeley, USA) make. $Hg[Co(NCS)_4]$ was used as a standard. Experimental susceptibility data were corrected for diamagnetic contributions.[57] The diamagnetic corrections were as -403.2×10^{-6}, -405.7×10^{-6} and -451.9×10^{-6} cm^3 mol^{-1} for the complexes **1–3**, respectively. The magnetic susceptibility data were analyzed using the van Vleck equation with the eigenvalues of the spin-coupling Hamiltonian ($\boldsymbol{H} = -2JS_1S_2$, $S_1 = S_2 = 5/2$). The coupling constants were obtained by non-linear fitting of the molar susceptibility data using the equation:

$$\chi = \frac{Ng^2\beta^2(2e^{2x} + 10e^{6x} + 28e^{12x} + 60e^{20x} + 110e^{30x})}{kT(1 + 3e^{2x} + 5e^{6x} + 7e^{12x} + 9e^{20x} + 11e^{30x})}$$

where χ is the molar magnetic susceptibility per iron and x is $-J/kT$.[58] The molar magnetic susceptibility was corrected for temperature independent paramagnetism. Molar conductivity measurements were done using a Control Dynamics (India) conductivity meter. Cyclic voltammetric measurements were made at 25 °C using EG & G PAR 253 VersaStat potentiostat/galvanostat with a three-electrode configuration consisting of a glassy carbon working, a platinum wire auxiliary and a saturated calomel reference (SCE) electrode. $K_4[Fe(CN)_6]$ as a standard gave $E_{\frac{1}{2}} =$ 0.21 V *vs.* SCE in H_2O–0.1 M KCl.

Preparation of $[Fe_2(\mu\text{-}O)(L\text{-his})_2(B)_2](ClO_4)_2$ (B: bpy, 1; phen, 2; dpq, 3)

The complexes were prepared by following a general procedure in which a 5 cm^3 methanolic solution of $NaClO_4$ (122 mg, 1 mmol) was added to a 10 cm^3 MeOH solution of $Fe(NO_3)_3 \cdot 9H_2O$ (404 mg, 1 mmol) followed by an addition of solid L-histidine (155 mg, 1 mmol). The solution turned greenish brown. A 5 cm^3 methanolic solution of the heterocyclic base (bpy, 156 mg; phen, 198 mg; dpq, 230 mg; 1 mmol) was added to isolate the product in ~70% yield (330 mg, **1**; 340 mg, **2**; 385 mg, **3**). The solid was purified by washing with MeCN followed by diethyl ether and finally dried in vacuum over P_4O_{10}.

Anal. calc. for $C_{32}H_{32}N_{10}O_{13}Cl_2Fe_2 \cdot 4H_2O$ (**1**·4H_2O): C, 37.7; H, 4.0; N, 13.7%. Found: C, 37.6; H, 3.8; N, 14.0%. FT-IR (KBr phase), cm^{-1}: 3440 br (H_2O), 3020 br (NH), 1620 s (C=O), 1380 s, 1087 vs (ClO_4^-), 942 w, 820 m, 757 m, 656 w, 630 m, 565 w, 532 w (br, broad; vs, very strong; s, strong; m, medium; w, weak). ESI-MS in H_2O: m/z 374 $[M - 2(ClO_4^-)]^{2+}$. UV-visible in Tris-HCl buffer [λ_{max}, nm (ε, dm^3 mol^{-1} cm^{-1})]: 264 (54900), 523 sh (270) (sh, shoulder). Λ_M (S m^2 mol^{-1}) in H_2O: 175. μ_{eff}: 2.91 μ_B/Fe at 298 K.

Anal. calc. for $C_{36}H_{32}N_{10}O_{13}Cl_2Fe_2 \cdot 2H_2O$ (**2**·2H_2O): C, 41.9; H, 3.5; N, 13.6%. Found: C, 41.7; H, 3.4; N, 13.8%. FT-IR (KBr phase), cm^{-1}: 3420 br (H_2O), 3025 br (NH), 1622 s (C=O), 1385 s, 1140 w, 1088 vs (ClO_4^-), 990 m, 830 m, 720 m, 630 m, 570 w. ESI-MS in H_2O: m/z 398 $[M - 2(ClO_4^-)]^{2+}$. UV-visible in Tris-HCl buffer [λ_{max}, nm (ε, dm^3 mol^{-1} cm^{-1})]: 280 (41730), 334 (7360), 519 sh (350) (sh, shoulder). Λ_M (S m^2 mol^{-1}) in H_2O: 190. μ_{eff}: 2.87 μ_B/Fe at 298 K.

Anal. calc. for $C_{40}H_{32}N_{14}O_{13}Cl_2Fe_2 \cdot 3H_2O$ (**3**·3H_2O): C, 41.7; H, 3.3; N, 17.0%. Found: C, 41.8; H, 3.0; N, 17.2%. FT-IR (KBr phase), cm^{-1}: 3402 br (H_2O), 3040 br (NH), 1620 s (C=O), 1480 w, 1380 s, 1088 vs (ClO_4^-), 980 w, 820 m, 730 w, 656 w, 630 m, 570 w. ESI-MS in H_2O: m/z 450 $[M - 2(ClO_4^-)]^{2+}$. UV-visible in Tris-HCl buffer [λ_{max}, nm (ε, dm^3 mol^{-1} cm^{-1})]: 253 (53790), 293 sh (22270), 326 (11050), 340 (9400), 517 sh (460). Λ_M (S m^2 mol^{-1}) in H_2O: 185. μ_{eff}: 2.83 μ_B/Fe at 298 K.

CAUTION! The perchlorate salts could be potentially explosive. Therefore, only small quantities of the sample was handled to avoid any possible explosion.

Solubility and stability

The complexes were soluble in water, dimethylformamide (DMF) and dimethyl sulfoxide (DMSO). The complexes were stable in the solid phase at ambient temperature in the light. The solutions on keeping for a long period in light gave a red solid of binary composition $[Fe^{II}(B)_3](ClO_4)_2$ as evidenced from the visible spectral band of the binary iron(II) complex.

X-Ray crystallographic procedure

The reddish brown rectangular shaped crystals of **1** were grown from an aqueous solution of **1** on slow evaporation. The crystal mounting was done on a glass fiber using epoxy cement. The X-ray diffraction data were measured in frames with increasing ω (width of 0.3° per frame) and with a scan speed at 15 s per frame using a Bruker SMART APEX CCD diffractometer, equipped with a fine focus 1.75 kW sealed tube X-ray source. Empirical absorption correction was made using multi-scan program.[59] The structure was solved by heavy-atom method and refined by full matrix least-squares using SHELX system of programs.[60] The perspective view of the complex was obtained using the ORTEP program.[61] There were two molecules in the crystallographic asymmetric unit of **1** in the monoclinic space group $C2$. While one ClO_4^- in **1** was refined with full atom occupancy, the other positionally disordered ClO_4^- was modeled for two ClO_4 units each refined with half-occupancy keeping the central Cl atom with full occupancy. The disordered perchlorate oxygen atoms were refined isotropically. The other non-hydrogen atoms were refined anisotropically. The hydrogen atoms were fixed in their calculated positions using a riding model. The CCDC number for the complex **1** is 678207.[33]

Crystal data for $\mathbf{1}\cdot 4H_2O$: $C_{32}H_{40}Cl_2Fe_2N_{10}O_{17}$, $M = 1019.34$, monoclinic, space group $C2$, $a = 18.265(3)$, $b = 12.584(2)$, $c = 19.116(3)$ Å, $\beta = 102.399(4)°$, $U = 4291.5(13)$ Å^3, $Z = 4$, $D_c = 1.578$ Mg m^{-3}, $T = 293(2)$ K, $1.09 \leq \theta \leq 25.00°$, $\mu = 8.83$ cm^{-1}, $F(000) = 2096$, GOF = 1.042, $R_1 = 0.1218$, w$R_2 = 0.2928$ for 7441 reflections with $I > 2\sigma(I)$ and 568 parameters [$R_1(F^2) = 0.1849$ (all data)]. Weighting scheme: $w = [\sigma^2(F_0^2) + (0.1480P)^2 + 0.000P]^{-1}$, where $P = [F_0^2 + 2F_c^2]/3$.

DNA binding experiments

DNA binding propensities of the complexes were investigated using various spectroscopic, isothermal titration calorimetric and viscometric titration techniques. UV-visible titration experiments were carried out in Tris-HCl/NaCl buffer (5 mM Tris-HCl/NaCl, pH 7.2) using aqueous solutions of the complexes. Calf thymus (CT) DNA (*ca.* 130 μM NP) in Tris-HCl buffer medium was found to be free from any protein impurity as evident from the ratio of UV absorbance at 260 and 280 nm of *ca.*1.9 : 1. The CT DNA concentration was measured from its absorption intensity at 260 nm using molar absorption coefficient value of 6600 dm^3 mol^{-1} cm^{-1}.[62] UV-visible absorption titration experiments were performed with increasing concentrations of CT DNA keeping the complex concentration as constant at 30 μM. Due correction was made to the absorbance of CT DNA itself. Samples were initially pre-equilibrated with CT DNA for 5 min before recording each spectrum. The equilibrium binding constant (K_b) and the binding site size (s) of the complex as a fitting parameter were determined from a non-linear fitting of the plot of $\Delta\varepsilon_{af}/\Delta\varepsilon_{bf}$ *vs.* [DNA] applying McGhee–von Hippel (MvH) method and using the expression of Bard and coworkers: $\Delta\varepsilon_{af}/\Delta\varepsilon_{bf} = (b - (b^2 - 2K_b^2C_t[DNA]/s)^{\frac{1}{2}})/2K_b$, $b = 1 + K_bC_t + K_b[DNA]/2s$, where K_b is the microscopic equilibrium binding constant for each site, C_t is the total concentration of the metal complex, s is the site size of the metal complex interacting with the DNA, [DNA] is the concentration of DNA in nucleotides, ε_f, ε_a and ε_b are respectively the molar extinction coefficient values of the free complex in solution, complex bound to DNA at a definite concentration and the complex in completely bound form with CT DNA.[63,64] The non-linear least-squares analysis was done using Origin Lab, version 7.0.

The apparent binding constant (K_{app}) values of the complexes were determined by ethidium bromide (EB) displacement assay using EB bound CT DNA solution in 5 mM Tris-HCl/NaCl buffer (pH 7.2). The fluorescence intensities of EB at 600 nm (546 nm excitation) with increasing complex concentration were measured. EB did not show any fluorescence in Tris buffer medium.[65] It, however, showed enhanced emission intensity in the presence of CT DNA due to its intercalative binding to DNA. Competitive binding of the oxo-bridged diiron(III) complexes to CT DNA showed a gradual decrease in the emission intensity of EB. The relative binding order was obtained from the comparison of the slopes of the I/I_0 *vs.* [complex] plots.

DNA melting experiments were carried out by monitoring the absorbance of the CT DNA (260 nm) in the temperature range of 40 to 90 °C in absence and in the presence of the complexes in a 13 : 1 molar ratio of the CT DNA and the complex with a ramp rate of 0.5 °C min^{-1} in 5 mM phosphate buffer medium (pH 6.85) using Cary 300 bio UV-Vis spectrometer with Cary temperature controller. The melting of the double-strand DNA to single-strand DNA was observed with a significant hyperchromicity of the absorbance at 260 nm. The melting temperature was determined from the derivative plot (dA_{260}/dT *vs.* T) of the melting profile. Viscometric titration experiments were done using Schott Gerate AVS 310 automated viscometer attached with constant temperature bath at 37 °C to determine the nature of the interaction of the complexes with the CT DNA. The concentration of CT DNA stock solution was 130 μM (NP) in 5 mM Tris-HCl buffer. The complex was added gradually in increasing concentration from 0 to 250 μM and the viscosity was measured after each addition. The flow times were monitored with an automated timer. The data were presented by ploting relative specific viscosity of DNA, $(\eta/\eta_0)^{1/3}$ *vs.* [complex]/[DNA], where η is the viscosity of DNA in the presence of the complex and η_0 is the viscosity of DNA alone in 5 mM Tris buffer medium. The viscosity values were calculated from the observed flow time of CT DNA containing solutions (t) duly corrected for that of the Tris buffer alone (t_0), $\eta = (t - t_0)$.[66]

Isothermal titration calorimmetric (ITC) experiments were performed using Nano-Isothermal Titration Calorimeter III, Model CSC 5300. In a typical experiment, a 1.0 cm^3 solution of CT-DNA in 5 mM Tris-HCl/25 mM NaCl buffer was placed in the sample cell of the calorimeter and equilibrated to 20 °C for 3 h before performing the experiment. A 100 μM CT DNA

was used for the titration against the complexes (2 mM). The complex solution that was placed in the injection syringe of 250 μL was injected into the sample cell in 31 injections with 8 μL per injection. Control titration experiments of the complex into the 5 mM Tris-HCl/25 mM NaCl buffer were also performed in order to subtract background heat of dilution that was found to be insignificant from the ITC data. The data were fitted to single set of binding site model using the Bind Works, version 3.1.11 software package.[67]

Molecular docking

Molecular docking was performed using the DS Modeling 1.2-SBD Docking Module by Accelrys™ Software.[68] The CHARMm force-field was used for the metal complex in the input of the calculations. Due to the higher hybridization state of Fe^{3+} atom in the molecule, the correction of the partial charge distribution for all atoms in the ligand was done by following the output from Gaussian 03.[69] The crystal structure of the B-DNA dodecamer $d(CGCGAATTCGCG)_2$ (NDB code GDLB05) was downloaded from the protein data bank. In the docking analysis, the binding site was assigned across the entire minor and major grooves of the DNA molecule. The docking was performed to find the most stable and favorable orientation (*vide* ESI†).

Protein binding experiments

The protein binding propensity of the complexes was determined by tryptophan fluorescence quenching experiment as well as by isothermal titration calorimetry using bovine serum albumin (BSA) protein as the substrate. In a typical tryptophan fluorescence quenching experiment in phosphate buffer (pH 6.8), quenching of the emission intensity of tryptophan residues (trp-134 and trp-214) of BSA at 344 nm (excitation wavelength at 295 nm) was monitored using complexes **1–3** with increasing complex concentration.[70] The Stern–Volmer (I_0/I) *vs.* [complex] plots using the corrected fluorescence data that took into account the effect of dilution were done. Linear fit of the Stern–Volmer equation ($I_0/I = 1 + K_{BSA}[Q]$), where I_0, I are respective emission intensity of BSA in the absence of the quencher and emission intensity of BSA in the presence of the quencher of concentration [Q] gave the binding constant (K_{BSA}) value using Origin 7.0.

Isothermal titration calorimetry for BSA binding was performed in a similar way as was done for the CT DNA. BSA, at a concentration of 100 μM in 5 mM Tris-HCl/25 mM NaCl (pH 7.2), was placed in the 1.4 cm^3 calorimeter cell and the complex (2 mM) was added gradually in 8 μL aliquots for each injection for a total of 31 injections at 5 min intervals. The heat of reaction per injection was determined by integration of the peak areas using the Bind Works, version 3.1.11 software package.[67] The plots of the heat evolved per mol complex injected *vs.* the complex/BSA molar ratio was fitted into the single set binding site model. The best-fit values of the heat of binding (ΔH), the stoichiometry of binding (N), and the binding constant (K) were obtained from the same plot. The heats of dilution were taken into account from a control experiment that was done by injecting 2 mM complex into the buffer solution. The heats of dilution were subtracted from the corresponding complex/BSA binding experiment data before curve-fitting.

DNA cleavage experiments

The supercoiled (SC) pUC19 DNA (1 μL, 0.2 μg, 30 μM, 2686 base pairs) cleavage activity of **1–3** was studied by agarose gel electrophoresis in 50 mM Tris-HCl/NaCl buffer (pH 7.2). The chemical nuclease activity of the complexes was studied using 3-mercaptopropionic acid (MPA, 500 μM) as a reducing agent in dark. The photo-induced DNA cleavage reactions were performed under illuminated conditions using UV-A lamp of 365 nm (6 W, sample area of illumination: 45 mm^2) and at different visible wavelengths (458, 520 and 647 nm) using a continuous-wave (CW) argon–krypton laser (50 mW laser power, laser beam diameter of 1.8 mm with a beam divergence of 0.70 mrad) of the Spectra Physics Water-Cooled Mixed-Gas Ion Laser Stabilite® 2018-RM model. The power of the Ar–Kr laser beam at the sample position (~5 mm away from the laser source) was measured using Spectra Physics CW Laser Power Meter (Model 407A). Eppendorf and glass vials were used for respective UV-A and visible light experiments in a dark room at 25 °C.

The anaerobic photocleavage experiment was performed under argon atmosphere. Different additives like singlet oxygen quenchers and radical scavengers were used for mechanistic investigations in the presence of the complexes. The concentrations of the complexes and the additives corresponded to the quantity in 2 μL stock solution after dilution to the 20 μL final volume using Tris-HCl/NaCl buffer. After the photoexposure, the sample was incubated for 1 h at 37 °C, followed by its addition to the loading buffer containing 25% bromophenol blue, 0.25% xylene cyanol and 30% glycerol (2 μL). The solution was finally loaded on 0.8% agarose gel containing 1.0 μg mL^{-1} EB. Electrophoresis was carried out in a dark room for 2 h at 45 V in Tris–acetate–EDTA (TAE) buffer. The bands were visualized by UV light and photographed. The extent of DNA cleavage was determined by measuring the intensities of the bands using a UVITECH Gel Documentation System. Due corrections were made to the intensity data for the presence of minor quantity of nicked circular (NC) DNA in the original SC DNA sample and for the low affinity of EB binding to SC compared to NC and linear forms of DNA.[71] The extent of experimental error in measuring the SC and NC forms of DNA from the gel diagrams varied from 3–5%.

Protein cleavage experiments

Photo-induced protein cleavage experiments were carried out according to the literature procedure described by Kumar and coworkers.[72] Freshly prepared solution of BSA in 50 mM Tris-HCl buffer (pH 7.2) was used for the photo-induced protein cleavage studies. The protein (2.5 μM) solutions in Tris-HCl buffer medium containing complexes with varied concentration from 50–200 μM were photo-exposed at 365 nm (100 W) for 20 min and eppendorf vials were used for the UV-A light-induced protein cleavage studies. The sample solutions were incubated at 37 °C for 1 h prior to the photoexposure. The irradiated samples (50 μL) were dried in EYELA centrifugal vaporizer (Model CVE-200D) and the samples were dissolved in the loading buffer (24 μL) containing SDS (7% w/v), glycerol (4% w/v), Tris-HCl buffer (50 mM, pH 6.8), mercaptoethanol (2% v/v) and bromophenol blue (0.01% w/v). The protein solutions were then denatured on heating to boil. Samples were then loaded

on a 3% polyacrylamide (stacking) gel. The gel electrophoresis that was done initially at 60 V until the dye passed into the separating gel (10% polyacrylamide) from the stacking (3%) gel, followed by setting the voltage to 110 V for 1.5 h. Staining was done with Coomassie Brilliant Blue R-250 solution (acetic acid–methanol–water = 1 : 2 : 7 v/v) and destaining was done with water–methanol–acetic acid mixture (5 : 4 : 1 v/v) for 4 h. The gels, after destaining, were scanned with a HP Scanjet G3010 scanner and the images were further processed using Adobe Photoshop 7.0 software package. Molecular weight markers were used in each gel to calibrate the molecular weights of the BSA. The presence of reactive oxygen species was investigated by carrying out the photo-induced protein cleavage experiments in the presence of various singlet oxygen quenchers like NaN_3 (3 mM), TEMP (3 mM) and hydroxyl radical scavengers like DMSO (20 μL), KI (3 mM) and mannitol. The photocleaved BSA was dialyzed using dialysis tube (cut-off 3 kDa) to isolate the sample containing protein fragments for mass spectral study to determine the molecular weight of the fragments.

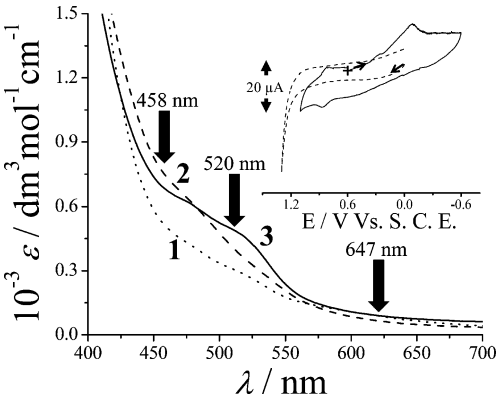

Fig. 2 Visible electronic spectra of the complexes **1–3** in Tris-HCl buffer showing the LMCT band near 500 nm. The arrows indicate the visible wavelengths used in the DNA photocleavage studies. The inset shows an irreversible cyclic voltammetric responses observed for **3** in H_2O–0.1 M KCl at 50 mV s^{-1}. The dashed line show the anodic scan for **3**.

Results and discussion

Synthesis and general aspects

Three (μ-oxo)diiron(III) L-histidine complexes $[\{Fe(L\text{-}his)(B)\}_2(\mu\text{-}O)](ClO_4)_2$ (**1–3**) were prepared in good yield from the reaction of $Fe(NO_3)_3{\cdot}9H_2O$ with the amino acid and the heterocyclic base in methanol (B: bpy, **1**; phen, **2**; dpq, **3**). The products were isolated as the perchlorate salt. The complexes were characterized from analytical, spectral and magnetic data (Table 1, ESI Fig. S1–S6†). The IR spectra of the complexes displayed characteristic $\nu(ClO_4^-)$ at ~1088 cm^{-1} and ν(C=O) at ~1630 cm^{-1}. The variable-temperature magnetic susceptibility data showed strong antiferromagnetic coupling between the metal centers through the oxo-bridge giving a $-J$ value of ~110 cm^{-1} (ESI Fig. S5†).[73] The electronic spectra of the complexes in Tris-HCl buffer medium (pH 7.2) exhibited weak oxo→Fe(III) charge transfer band at ~520 nm and the ligand centered electronic bands in the UV region (Fig. 2, ESI Fig. S4†). The spectral bands near 350 nm are assignable to the n–π* and/or π–π* electronic transitions of the quinoxaline moiety of the dpq ligand in **3**.[74] The redox properties of the complexes were investigated by cyclic voltammetry in H_2O–0.1 M KCl (Table 1). The complexes showed irreversible cathodic response with a peak current that corresponds to two-electron reduction of the $\{Fe^{III}{}_2O\}$ unit near –0.1 V *vs.* SCE without showing any anodic counterpart. The dpq complex **3** showed ligand reductions in the potential range of –1.0 to –1.8 V. A quasi-reversible cyclic voltammetric response was observed at ~1.0 V for the complexes after making the initial cathodic scan. This redox response is believed to be due to the formation of stable binary monomeric iron(II) species $[Fe(B)_3]^{2+}$ from degradation of the unstable reduced $\{Fe^{II}\text{–}O\text{–}Fe^{II}\}$ core. Such redox behaviour has been found to be common for the oxo-bridged diiron(III) complexes having phenanthroline bases.[75] The anodic voltammetric response is, however, not observed during an initial anodic scan within the voltage window of 0.0 to 1.3 V *vs.* SCE (Fig. 2).

X-Ray crystallography

The bipyridyl complex **1** has been structurally characterized by single crystal X-ray diffraction technique. Complex **1** crystallized in *C*2 space group in the monoclinic crystal system with four molecules in the unit cell. An ORTEP view of the cationic complex is shown in Fig. 3. Selected bond distances and angles data are given in Table S1 (*vide* ESI†). The unit cell packing diagram is shown in Fig. S7 (*vide* ESI†). The complex has a (μ-oxo)diiron(III)

Table 1 Selected physicochemical and DNA binding data for the complexes **1–3**

Complex	**1**	**2**	**3**
IR:[a] ν (ClO_4^-)/cm^{-1}	1085	1088	1089
Electronic spectra:[b] λ_{max}/nm (ε/dm^3 mol^{-1} cm^{-1})	523 sh (270)	519 sh (350)	517 sh (460)
Conductivity:[b] Λ_M/S m^2 mol^{-1}	175	190	185
Cyclic voltammetry:[c] E_{pc}/V (*vs.* SCE)	–0.25	–0.08	–0.05
Magnetism:[d] $-J$/cm^{-1}	112	110	108
K_{app}[e]/M^{-1}	4.6×10^5	2.6×10^6	6.6×10^6
K_b[f]/M^{-1} [*s*]	$4.6\ (\pm0.5) \times 10^4$ [0.25]	$1.1\ (\pm0.6) \times 10^5$ [0.22]	$5.6\ (\pm0.7) \times 10^5$ [0.2]
ΔT_m[g]/°C	1	2.3	4.5
K_{BSA}[h]/M^{-1}	3.6×10^4	5.7×10^4	8.8×10^4

[a] KBr phase. [b] In H_2O. sh, shoulder. [c] Fe(III)/Fe(II) cathodic peak in aqueous medium with 0.1 M KCl as supporting electrolyte. Scan rate = 50 mV s^{-1}. [d] Magnetic exchange parameter. [e] Apparent binding constant determined from ethidium bromide displacement assay. [f] Equilibrium DNA binding constant and *s* is the binding site size determined from the UV-visible absorption spectral titration. [g] Change in DNA melting temperature. [h] Stern–Volmer fluorescent quenching constant determined from tryptophan fluorescent quenching experiment.

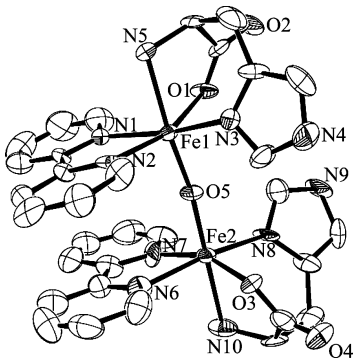

Fig. 3 ORTEP view of the cationic complex in **1** with 50% probability thermal ellipsoids and the atom numbering scheme for the metal and hetero atoms.

core with each iron bound to a NNO-donor L-histidine and NN-donor 2,2′-bipyridine giving a FeN_4O_2 coordination geometry. The Fe–O–Fe angle of 171.8(5)° is essentially linear. The average Fe–O distance is 1.78 Å. The bpy ligands in the solid state structure show a π–π stacking interaction in the *syn*-conformation.

DNA binding studies

The binding propensity of the complexes **1–3** to CT DNA was studied using different spectral techniques, viscometric titration experiments and by ITC method. The DNA binding data are tabulated in Tables 1 and 2. UV-visible absorption titration experiments were performed to determine the equilibrium binding constant (K_b) and the binding site size (s) of the complexes to the CT DNA. The intensity of the absorption band at ~290 nm was monitored for **1** and **2**, while the band at 340 nm was used for **3**. All the complexes showed minor bathochromic shift of ~2 nm of the band with significant hypochromicity of ~25% indicating appreciable groove/surface binding propensity of the complexes to the CT DNA (ESI Fig. S8†). The equilibrium binding constant (K_b) and the binding site size (s) values are ~10^5 M^{-1} and ~0.2, respectively, for complexes **2** and **3**. The bpy complex **1** displayed poor binding propensity to CT DNA. The dpq analogue showed significantly higher DNA binding possibly due to the presence of the quinoxaline ring favoring partial intercalation into the DNA bases through its extended planar aromatic ring. The low value of s is indicative of more surface aggregation and/or groove binding than any intercalation to the DNA base pairs.[76] The ethidium bromide displacement assay was used to study the relative binding of the complexes to CT-DNA. The emission intensity of EB was used as a spectral probe as EB showed reduced or no emission intensity in buffer solution because of solvent quenching and the emission intensity was significantly enhanced when EB intercalatively binds to DNA. The competitive binding of the complexes to DNA decreased the emission intensity of EB. The relative binding propensity of the complexes to DNA was measured from the extent of reduction of the emission intensity (ESI Fig. S9†). The apparent binding constant (K_{app}) values for **1–3** gave the order: **3** > **2** > **1**.

Table 2 Thermodynamic data for DNA and BSA binding by complexes **1–3** from ITC measurements

	1	**2**	**3**
DNA binding			
N^a	0.31	0.27	0.26
K^b/M^{-1}	3.52×10^4	1.46×10^5	4.55×10^5
ΔH^c/kJ mol^{-1}	–43.7	–59.5	–71.3
ΔG^d/kJ mol^{-1}	–25.5	–28.5	–39.5
$T\Delta S^e$/kJ mol^{-1}	18.2	31.0	39.8
BSA binding			
N^a	2.53	2.41	2.71
K^b/M^{-1}	2.4×10^4	4.2×10^4	5.8×10^4
ΔH^c/kJ mol^{-1}	–37.2	–39.8	–44.3
ΔG^d/kJ mol^{-1}	–24.6	–25.9	–26.7
$T\Delta S^e$/kJ mol^{-1}	12.6	13.9	17.6

[a] The binding stoichiometry (N) determined from the ITC data. [b] Bindnig constant obtained from the ITC experiments. [c] The enthalpy change in DNA binding. [d] Change in Gibb's free energy. [e] ΔS, change in entropy at 293 K.

The DNA denaturation experiment was performed to understand the nature of DNA binding of the complexes. A minor shift of ~1 °C was observed in the CT DNA melting temperature (T_m) in the presence of **1** indicating mainly surface aggregation or electrostatic interaction of the bpy complex to the CT DNA. Complexes **2** and **3** showed significant DNA groove binding with partial intercalation as evidenced from the higher ΔT_m values of 2.3 °C for **2** and 4.5 °C for **3** (Fig. 4(a)). The ΔT_m value for EB was found to be 8.2 °C. The DNA binding nature of the complexes was studied by viscometric titration method. The plot of $(\eta/\eta_0)^{1/3}$ *vs.* [complex]/[DNA] gives a measure of the viscosity changes (Fig. 4(b)). Classical intercalators like EB are known to increase the base pair separation resulting an increase in the relative viscosity of the DNA. In contrast, groove or surface binding can cause an increase in the effective length of DNA leading to a minor increase in the relative viscosity of the DNA solution.[77] Complexes **2** and **3** showed minor increase in the viscosity of CT-DNA suggesting primarily groove binding nature of the complexes though partial intercalation to the CT-DNA is likely for **3**.

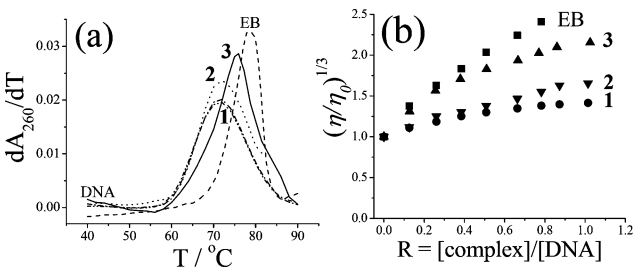

Fig. 4 (a) The CT DNA (130 μM) melting plots in absence (–···–) and presence of the complexes **1** (---), **2** (···), **3** (—) and EB (---) ([complex], 10 μM; [EB], 10 μM). (b) The effect of addition of EB (■), **1** (●), **2** (▼), and **3** (▲) on the relative viscosity of 130 μM CT DNA in 5 mM Tris-HCl buffer at 37 °C.

To further investigate the binding properties of the oxo-bridged diiron(III) complexes to the CT DNA, isothermal titration calorimetric study was done (Fig. 5, ESI Fig. S10(a)†). The binding isotherms fitted well with the single set of identical binding sites model. The thermodynamic profile for binding of the complexes displayed negative enthalpy and positive entropy changes indicating groove and/or partial intercalative binding being dominated by mainly hydrophobic interactions (Table 2).

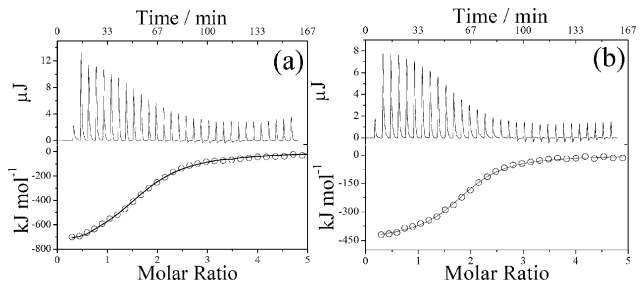

Fig. 5 Raw ITC data (top) and the integrated heat data with respect to time (bottom) for the interaction of the complexes **2** (a) and **3** (b) with the CT DNA in 5 mM Tris-HCl/25 mM NaCl buffer (pH 7.2). The ITC data were corrected for the dilution of the complexes using the buffer. The ITC data for the bpy complex **1** are given in ESI Fig. S10(a).†

Negative free energy change observed for the complexes on binding to the CT DNA suggest that the binding is energetically feasible with the binding order of ~10^5 M^{-1} except for the complex **1**, which showed relatively lower binding affinity with the order of ~10^4 M^{-1}. The dpq complex **3** showed highest binding propensity that is entropically driven as is evident from the large positive entropy change. The positive entropy change could be due to the π-stacking interactions of the planar phenanthroline bases (phen or dpq) into the DNA base pair in an interior hydrophobic medium of DNA causing significant release of the counter ions, *viz.* Na^+ into the bulk of the solvent.[78] This entropy effect for **3** was found to be more as the hydrophobicity of the dpq ring could displace a large number of Na^+ ions or water molecules into the bulk leading to more positive entropy. ITC data revealed the CT DNA binding order: **3** > **2** > **1**. The binding data, obtained from the ITC study, compared well with the K_b and K_{app} values obtained from the spectral measurements.

Molecular docking

The optimum docking states with the highest stabilization energy were obtained in a two stage docking. After the initial stage involving thorough analysis of different docked poses and the corresponding ligand conformations, the second stage of docking was performed in an energy profile guided manner depending upon the best binding trends using the top scored conformations of the ligand obtained as outputs from the first stage docking. Finally, the most favorable docked poses for the complexes **1–3** were obtained, as shown in Fig. 6 and ESI Fig. S11,† giving calculated free energy values of −4.71, −5.43 and −6.25 kcal mol^{-1}, respectively, with corresponding Ludi scores of 345.24, 398.2 and 458.6. Analysis of final docked poses of complexes **1–3** revealed an interesting trend in their DNA binding approach through the minor groove. There is an increasing order of binding from complex **1** to complex **3**, which is supported by the experimental DNA binding data as well.

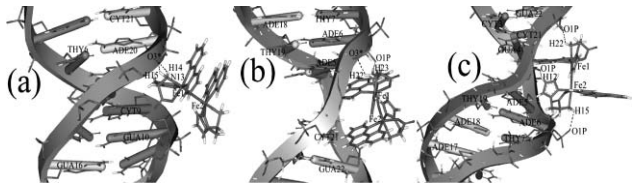

Fig. 6 Interaction of the complexes **1** (a), **2** (b) and **3** (c) with the $d(CGCGAATTCGCG)_2$ strands of DNA by formation of hydrogen bonds through its minor groove binding approach. Corresponding hydrogen bonds are shown as dotted lines. Detailed hydrogen-bonding parameters are given in Table 3.

Binding pose analysis and interactions with DNA in docked state showed that the binding energy is mainly derived from the H-bonding interactions with the phosphate backbone of DNA (Table 3). Additional stabilization came from partial aromatic stacking and hydrophobic surface complementarities of the complexes with the DNA bases (except for bpy complex **1**). Optimal binding conformation for the complexes **2** and **3** acquired a flipped conformation of the aromatic ring systems. In the case of **2**, two phenanthroline rings flipped apart partially, whereas complex **3** with two dpq rings flipped apart almost completely from the *syn* to *anti* conformation and hence provided a better scaffold for aromatic stacking interactions (Fig. 6). A detailed analysis of the docked structure thus revealed the necessity of the flipped state of the complex **3** as without this, due to steric hindrance, the docking could not be optimal. In the original state reported from the energy minimized model on the basis of crystal structure of complex **1**, the separation between the two planar dpq ligands is clearly inadequate for incorporation into the DNA base steps allowing the optimal binding interaction. The partial stacking information found from the docking study has been supported by the experimental evidence of DNA melting point elevation in the presence of **3**.

Table 3 Hydrogen bonding data for different docked poses of **1–3** with $d(CGCGAATTCGCG)_2$

For the docked pose of 1		
Donor group (Y–H)	Acceptor group Z	Distance [Y → Z]
N13–H14 (ligand)	O3* ADE19 (DNA-Chain B)	2.48 Å (bifurcated H-bond)
N13–H15 (ligand)	O3* ADE19 (DNA-Chain B)	2.48 Å (bifurcated H-bond)
For the docked pose of 2		
Donor group (Y–H)	Acceptor group Z	Distance [Y → Z]
N21–H22 (ligand)	O3* ADE5 (DNA-Chain A)	2.81 Å
N11–H23 (ligand)	O1P ADE6 (DNA-Chain A)	2.42 Å
For the docked pose of 3		
Donor group (Y–H)	Acceptor group Z	Distance [Y → Z]
N21–H22 (ligand)	O1P GUA22 (DNA-Chain B)	2.54 Å
N11–H12 (ligand)	O1P CYT21 (DNA-Chain B)	2.79 Å
N13–H15 (ligand)	O1P THY7 (DNA-Chain A)	3.49 Å

Chemical nuclease activity

The oxo-bridged diiron(III) complexes showed cleavage of pUC19 DNA (0.2 μg, 30 μM) in 50 mM Tris-HCl/50mM NaCl buffer (pH 7.2) in the presence of 500 μM 3-mercaptopropionic acid (MPA) as a reducing agent (Fig. 7). The extent of DNA cleavage by the complexes as observed from the agarose gel electrophoresis followed the DNA binding propensity of the complexes. A 30 μM concentration of **3** showed complete cleavage of SC DNA to its nicked circular (NC) form. The phen complex also showed similar chemical nuclease activity. The bpy complex was found to be chemical nuclease inactive because of its inability to bind to the DNA. Control experiments using only 500 μM MPA or the complexes (30 μM) alone did not show any DNA cleavage activity. The precursor species $Fe(NO_3)_3{\cdot}9H_2O$ in the presence of MPA did not show any DNA cleavage activity.

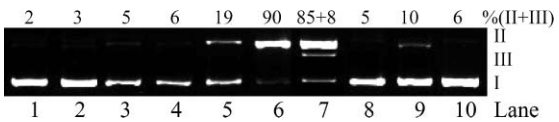

Fig. 7 Gel electrophoresis diagram showing the chemical nuclease activity of the complexes (30 μM) using SC pUC19 DNA (0.2 μg, 30 μM bp) in the presence of 500 μM MPA: lane 1, DNA control; lane 2, DNA + MPA; lane 3, DNA + **2**; lane 4, DNA + **3**; lane 5, DNA + **1** + MPA; lane 6, DNA + **2** + MPA; lane 7, DNA + **3** + MPA; lane 8, DNA + distamycin-A (100 μM) + MPA; lane 9, DNA + distamycin-A (100 μM) + **2** + MPA; lane 10, DNA + distamycin-A (100 μM) + **3** + MPA.

The reactive species involved in the DNA cleavage reaction is believed to be a two-electron reduced complex with a (μ-oxo)diiron(II) core in DNA-bound form. The cyclic voltammetric study on the diiron(III) complexes in absence of DNA showed the formation of inactive $[Fe(B)_3]^{2+}$ species on a cathodic scan. A similar observation was made from the reaction of the diiron(III) complexes with MPA in absence of DNA showing the appearance of a visible spectral band of $[Fe(B)_3]^{2+}$.[30] The monomeric iron(II) complexes of phenanthroline bases were, however, found to be chemical nuclease inactive.[30b] To circumvent the problem associated with the degradation of the (μ-oxo)diiron(III) core in the presence of a reducing agent, the SC DNA was incubated with the complexes for 1 h prior to the addition of MPA.

To explore the DNA groove binding preference of the complexes, the DNA cleavage activity of the complexes was studied in the presence of DNA minor groove binder distamycin-A.[79] A significant inhibition in the DNA cleavage was observed suggesting minor groove binding propensity of the complexes (Fig. 7). Mechanistic aspects of the chemical nuclease activity were studied using different additives. Addition of singlet oxygen quenchers like NaN_3 or L-histidine did not show any apparent inhibition in the DNA cleavage activity but hydroxyl radical scavengers like DMSO, KI and catalase or superoxide dismutase (SOD) as superoxide scavenger showed significant inhibitory effect in the chemical nuclease activity (ESI Fig. S12†). The mechanistic data suggest that the DNA cleavage reaction of the complexes in the presence of MPA proceeds *via* hydroxyl radical pathway following the Fenton like chemistry in which the reduced iron centers in DNA-bound form could activate molecular oxygen to generate reactive superoxide and subsequently hydroxyl radical species.[80]

DNA photocleavage activity

Photo-induced DNA cleavage activity of the oxo-bridged diiron(III) complexes was studied using SC pUC19 DNA (0.2 μg, 30 μM) in 50 mM Tris-HCl/NaCl buffer (pH, 7.2) on irradiation with a monochromatic UV-A light of 365 nm (6 W) and visible light of wavelengths 458, 520 and 647 nm (50 mW) using a CW argon–krypton mixed gas ion laser. Complexes **2** and **3** showed efficient DNA cleavage activity in UV-A light (Fig. 8). The bpy complex **1** was cleavage inactive possibly due to its poor DNA binding propensity. The DNA cleavage activity at 365 nm follows the order: **3** > **2** >> **1**. A 5 μM concentration of **3** on 2 h of photoexposure showed essentially complete cleavage of SC DNA with significant amount of linear DNA formation (~40%) (lane 4, Fig. 8). Complex **2** showed similar cleavage activity (~90%), but with only DNA single-strand breaks (lane 3, Fig. 8). Control experiments revealed that $Fe(NO_3)_3{\cdot}9H_2O$, phen, dpq or L-histidine alone of 80 μM concentration did not show any significant photocleavage of DNA on photoexposure at this wavelength. Again, the complexes (40 μM) in the dark or under argon atmosphere were inactive thus ruling out the possibility of any hydrolytic cleavage of DNA. The photo-induced DNA cleavage activity of the phen and dpq complexes could be due to photo-decarboxylation of L-histidine involving the Fe(III)-carboxylate bond and the quinoxaline moiety of dpq in **3** having conjugated C=N bonds generating photoexcited $^3(n–\pi^*)$ and/or $^3(\pi–\pi^*)$ state(s) to activate molecular oxygen.[81]

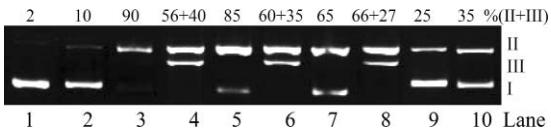

Fig. 8 Gel electrophoresis diagram showing the photo-induced SC pUC19 DNA (0.2 μg, 30 μM bp) cleavage activity of **1–3** (5 μM at 365 nm and 40 μM in visible light) with a photoexposure time of 2 h: lane 1, DNA control (λ, 365 nm); lane 2, DNA + **1** (λ, 365 nm); lane 3, DNA + **2** (λ, 365 nm); lane 4, DNA + **3** (λ, 365 nm); lane 5, DNA + **2** (λ, 458 nm); lane 6, DNA + **3** (λ, 458 nm); lane 7, DNA + **2** (λ, 520 nm); lane 8, DNA + **3** (λ, 520 nm); lane 9, DNA + **2** (λ, 647 nm); lane 10, DNA + **3** (λ, 647 nm). The laser power used was 50 mW using CW Ar–Kr laser.

Complexes **2** and **3** on photo-exposure to visible light showed significant DNA photocleavage activity (Table 4, Fig. 8). We selected 520 nm wavelength for photoactivation based on the metal-centered band near 520 nm in the complexes. Additionally, we explored DNA photocleavage activity at 647 nm that falls in the PDT spectral window. Complex **3** exhibited essentially complete cleavage of SC DNA on photoirradiation at both 458 and 520 nm (lanes 6 and 8, Fig. 8) with significant amount of linear DNA formation but showed less DNA cleavage (~35%) at 647 nm with no linear DNA (lane 10, Fig. 8). The extent of linear DNA formation was found to be more at shorter wavelengths, possibly due to photoactivation of the dpq ligand and photodecarboxylation of L-his in blue or UV-A light. The phen complex **2** also showed significant DNA cleavage activity on photoexcitation at 458 and 520 nm but less cleavage in red light with only single-strand breaks at all these wavelengths (lanes 5, 7, 9 in Fig. 8). The DNA double-strand breaks of DNA by **3** could be rationalized from the molecular docking calculations (Fig. 6). The complex was able to dock into the minor groove

Table 4 Selected photoinduced SC pUC19 DNA (0.2 μg, 30 μM bp) cleavage data for the complexes **1–3**

Sl. No.	Reaction conditions	λ^a/nm ([complex]/μM)	% (II + III)
1.	DNA control	365	2
2.	DNA + $Fe(NO_3)_3{\cdot}9H_2O^b$	365	4
3.	DNA + phen[b]	365	6
4.	DNA + dpq[b]	365	9
5.	DNA + L-histidine[b]	365	5
6.	DNA + **2**	In dark (40)	7
7.	DNA + **3**	In dark (40)	10
8.	DNA + **1**	365 (5)	10
9.	DNA + **2**	365 (5)	90
		458 (40)	85
		520 (40)	65
		647 (40)	25
10.	DNA + **3**	365 (5)	56 + 40
		458 (40)	60 + 35
		520 (40)	66 + 27
		647 (40)	35

[a] Wavelengths used for DNA photocleavage: $\lambda = 365$ nm (6 W UV lamp), $\lambda = 458$, 520 and 647 nm (CW Ar–Kr laser, 50 mW), [b] The concentration of $Fe(NO_3)_3{\cdot}9H_2O$, phen, dpq or L-histidine was 80 μM.

of the DNA by structural flipping of the dpq rings from *syn* to *anti* conformation around the linear Fe–O–Fe bond and was able to access both the strands for cleavage (chain A and chain B of the DNA dodecamer used for docking study). The inability of complex **2** to effect DNA double-strand breaks could be due to the presence of photo-inactive phen ligands.

The mechanistic aspects of the photo-induced DNA cleavage activity of the complexes **2** and **3** at 520 nm was investigated using various additives (Fig. 9). The complexes did not show any appreciable DNA photocleavage activity under argon suggesting the involvement of reactive oxygen species (ROS) in the DNA cleavage reactions. Addition of singlet oxygen quenchers like L-histidine, sodium azide (NaN_3) or TEMP under aerobic condition did not show any inhibitory effect on the DNA cleavage activity. The hydroxyl radical scavengers like KI, DMSO or catalase and superoxide radical scavenger superoxide dismutase (SOD), however, showed significant inhibition in the DNA cleavage activity of the complexes. The mechanistic data indicate

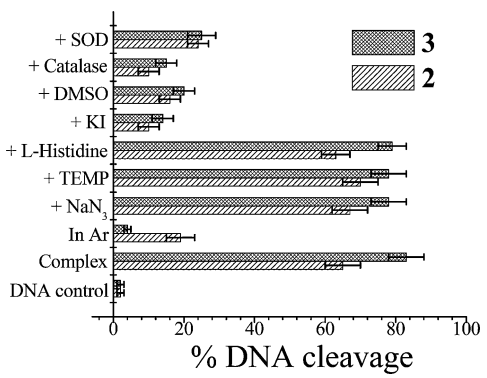

Fig. 9 The bar diagram showing mechanistic aspects of the visible light-induced SC pUC19 DNA (0.2 μg, 30 μM bp) cleavage activity of the complexes **2** and **3** in the presence of various additives (NaN_3, TEMP, L-his and KI of 500 μM; DMSO, 6 μL; catalase and SOD of 4 units). The wavelength used for 2 h photo-exposure of **2** and **3** (40 μM) was 520 nm.

the involvement of hydroxyl radical (•OH) as the DNA damaging agent.

Complex **3** in the absence of DNA, on photoexcitation at 365 nm under argon, showed the appearance of two intense bands at 512 and 475 nm that are assignable to the MLCT transitions of a binary dpq–iron(II) complex.[30] The binary complex was found to be photonuclease inactive in visible light. When **3** (0.4 mM) was photoexposed to 365 nm for 30 min in the presence of 5,5-dimethyl-1-pyrroline-*N*-oxide (DMPO, 20 mM) under aerobic condition, the formation of DMPO–•OH adduct was observed from the characteristic EPR signal of the species (Fig. 10). The a_N and a_H values of 14.5 and 14.6 G observed for the DMPO-stabilized hydroxyl radical compared well with the reported value of 14.9 G ($a_N = a_H$).[82]

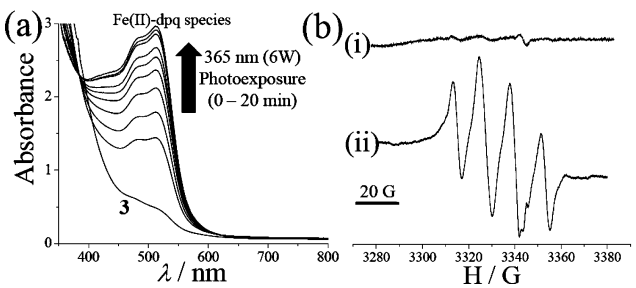

Fig. 10 (a) Spectral traces showing the enhancement of the Fe(II)–dpq (LMCT) band intensity on photoexposure of complex **3** (50 μM) at 365 nm for 20 min. (b) EPR spectra of complex **3** (0.4 mM) in the presence of DMPO (20 mM) in water before (i) and after (ii) photo-irradiation with UV-A light of 365 nm for 30 min.

The mechanistic data suggest a photo-redox pathway for the photo-induced DNA cleavage reactions of **2** and **3** in which photo-decarboxylation involving the Fe(III)–carboxylate(L-his) moieties reduce Fe(III) to Fe(II) which in turn reacts with molecular oxygen to produce superoxide radical and subsequently hydroxyl radical under aerobic conditions (Fig. 11).[30b,83]

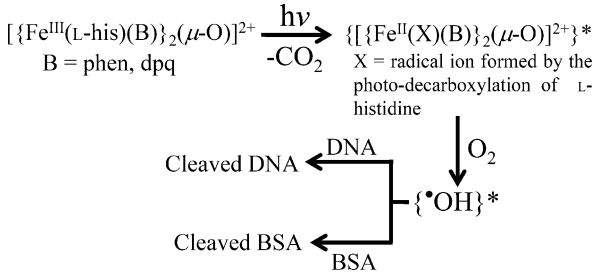

Fig. 11 The proposed photo-redox pathway involved in the oxidative cleavage of DNA or BSA by the complexes **2** and **3**.

BSA protein binding

The interaction of bovine serum albumin protein with the complexes **1–3** was investigated by tryptophan emission-quenching experiments. The fluorescence property of BSA in buffer medium is due to the presence of tryptophan residues (trp-134 and trp-214). The emission intensity of BSA was found to quench gradually on increasing the complex concentration because of changes in the secondary/tertiary structure of BSA in phosphate buffer medium

affecting the orientation of the tryptophan residues of BSA (ESI Fig. S13†). The extent of quenching of the fluorescence intensity of BSA gave the measure of extent of binding of the complexes to BSA. The dpq complex **3** gave the highest K_{BSA} value of 8.8×10^4 M^{-1}. The K_{BSA} values follow the order: **3** > **2** > **1** (Table 1). Complex **3** with its hydrophobic dipyridoquinoxaline ligand possibly increases the binding affinity in comparison to the other complexes.

The BSA binding propensity of the complexes was also studied by isothermal titration calorimmetric technique. The binding isotherms fitted well with the single set of identical binding sites model (Fig. 12, ESI Fig. S10(b)†). The binding stoichiometry was found to be ~2.5. The binding of the complexes were enthalpically and entropically favourable as evident from negative enthalpy and positive entropy values giving binding order of ~10^4 M^{-1}. The complex **3** showed higher binding propensity to BSA. The positive entropy change could be due to hydrophobic interactions involving the heterocyclic bases with the BSA causing significant release of the counter ions, *viz.* Na^+, into the bulk of the solvent.[78] This entropy effect for **3** was found to be more than for the other analogues. The binding data obtained from the ITC study compared well with the K_{BSA} values obtained from the tryptophan emission-quenching experiments.

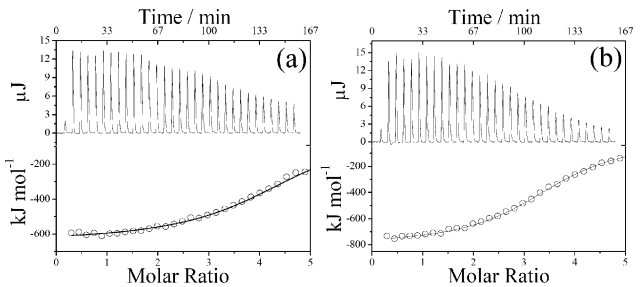

Fig. 12 Raw ITC data (top) and the integrated heat data with respect to time (bottom) for the interaction of the complexes **2** (a) and **3** (b) with bovine serum albumin (BSA, 0.1 mM) protein in 5 mM Tris-HCl/25 mM NaCl buffer (pH 7.2). The ITC data were corrected for the dilution of the complexes using the Tris buffer. The ITC data for the bpy complex **1** are given in ESI Fig. S10(b).†

BSA photocleavage activity

The BSA photocleavage activity of the complexes was studied using 4 μM BSA in 50 mM Tris-HCl buffer on exposure to UV-A light of 365 nm (100 W) with different complex concentrations and varied exposure times (5–20 min). The BSA cleavage activity was analysed by SDS-PAGE (Fig. 13, ESI Fig. S13†). Complex **1** was found to be cleavage inactive. Complex **2** showed minor cleavage activity. Complex **3** was found to be an efficient photocleaver of BSA in site-specific manner. The SDS-PAGE showed photo-products of BSA (66 kDa) with apparent molecular masses 45 kDa and 20 kDa. Two fragments seemed likely to arise from the same parent protein (BSA) from a single cut in the protein backbone. The complex **3** in dark did not show any photocleavage activity thus excluding the possibility of any hydrolytic cleavage of BSA. Similarly, irradiation of BSA in the absence of the metal complex did not yield any cleavage. Dose dependent photo-induced protease activity of the complex **3** (50–200 μM) against

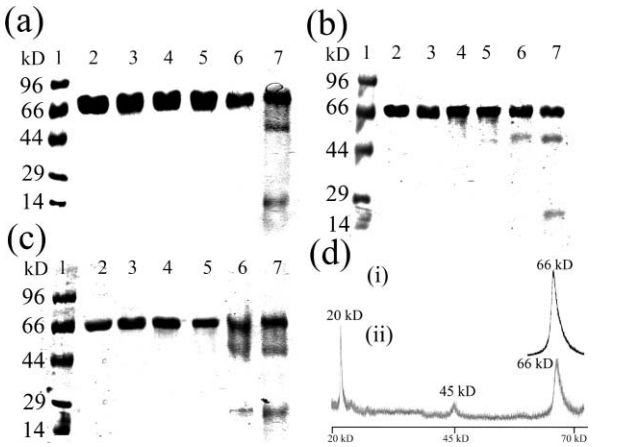

Fig. 13 (a) SDS-PAGE diagram showing oxidative cleavage of bovine serum albumin (BSA, 4 μM) protein in UV-A light of 365 nm (100 W lamp) by the complexes **1–3** in 50 mM Tris-HCl buffer (pH 7.2) for a photo-exposure time of 20 min: lane 1, molecular marker; lane 2, BSA control; lane 3, BSA + **2** (200 μM) in dark; lane 4, BSA + **3** (200 μM) in dark; lane 5, BSA + **1** (200 μM); lane 6, BSA + **2** (200 μM); lane 7, BSA + **3** (200 μM). (b) The SDS-PAGE diagram showing the dose dependence on the cleavage of BSA (4 μM) by **3** with 20 min photoexposure to UV-A light of 365 nm: lane 1, molecular marker; lane 2, BSA control; lane 3, BSA + **3** (25 μM); lane 4, BSA + **3** (50 μM); lane 5, BSA + **3** (100 μM); lane 6, BSA + **3** (150 μM); lane 7, BSA + **3** (200 μM). (c) SDS-PAGE diagram showing the time dependence on the photocleavage of BSA (4 μM) by **3** (200 μM): lane 1, molecular marker; lane 2, BSA control; lane 3, BSA + **3** (2 min); lane 4, BSA + **3** (5 min); lane 5, BSA + **3** (10 min); lane 6, BSA + **3** (15 min); lane 7, BSA + **3** (20 min). (d) MALDI-TOF MS plot of the dialyzed sample obtained from the photocleavage of BSA by **3** at 365 nm for an exposure time of 20 min showing formation of two fragments of 45 kDa and 20 kDa (ii) from BSA protein of 66 kDa (i).

4 μM BSA in Tris-HCl buffer medium was also studied. The extent of protein photocleavage was found to increase on increasing the concentration of the complex. The involvement of reactive oxygen species in the cleavage reaction was investigated using different additives (ESI Fig. S14†). Singlet oxygen quenchers like TEMP (3 mM) or NaN_3 (3 mM) did not show any apparent effect on photo-induced protein cleavage activity of **3**. Hydroxyl radical scavengers like KI (3 mM) and ethanol (30 μM) showed significant reduction in the photo-induced protease activity of **3** indicating the involvement of hydroxyl radicals as the reactive species. Metal based compounds are known to cleave BSA in site-specific manner primarily by hydrolytic pathway.[5,84] The complexes that show photo-induced site-specific oxidative cleavage of BSA are relatively rare in the literature.[9,50]

Conclusions

The oxo-bridged diiron(III) complexes having bio-essential L-histidine and N,N-donor heterocyclic bases form a new class of complexes showing novel photo-induced DNA and protein cleavage activity. The ITC data suggest single set of identical binding mode to bind with CT DNA with partial intercalative minor groove binding propensity of the phen and dpq complexes. Molecular docking calculations showed chemically significant flipping around Fe–O–Fe bond thus making both the strands accessible for cleavage. Complexes **2** and **3** showed chemical

nuclease activity in the presence of a reducing agent (MPA) and significant photo-induced DNA cleavage activity in UV-A and visible light. Significant results of this study include double strand DNA cleavage activity of complex **3**, significant photo-induced DNA cleavage activity within the PDT window by **2** and **3**, rationalization of the DNA double-strand breaks from theoretical calculations and photo-induced site-specific BSA cleavage activity of complex **3**. The DNA photocleavage activity presumably occurs from a photodecarboxylation process involving the carboxylate moiety of the metal-bound L-histidine ligand. The reaction seems to follow a photo-redox pathway generating reactive Fe(II) centers forming hydroxyl radicals under aerobic medium thus modeling the Fe(II)–bleomycin activity. The results are of importance in designing new iron-based synthetic photonucleases and photoproteases having bio-essential amino acids/peptides for potential applications in PDT and as anti-metastasis agents targeting both primary and secondary tumors.

Acknowledgements

We thank the Department of Science and Technology (DST), Government of India, and the Council of Scientific and Industrial Research (CSIR), New Delhi, for financial support [SR/S5/MBD-02/2007 and 01(2081)/06/EMR-II]. We also thank the Alexander von Humboldt Foundation, Germany, for donation of an electroanalytical system. We sincerely thank Prof. S. Ramakrishnan of our department for providing the ITC facility and Mr Ritankar Majumdar of the department of Molecular Reproduction, Development and Genetics for protein dialysis study. TB is thankful to CSIR for research fellowship. ARC thanks DST for J. C. Bose Fellowship.

References

1 (*a*) D. S. Sigman, A. Mazumder and D. M. Perrin, *Chem. Rev.*, 1993, **93**, 2295; (*b*) D. S. Sigman, *Acc. Chem. Res.*, 1986, **19**, 180.
2 L. K. J. Boerner and J. M. Zaleski, *Curr. Opin. Chem. Biol.*, 2005, **9**, 135.
3 G. Pratviel, J. Bernadou and B. Meunier, *Angew. Chem., Int. Ed. Engl.*, 1995, **34**, 746.
4 C. Metcalfe and J. A. Thomas, *Chem. Soc. Rev.*, 2003, **32**, 215.
5 H. T. Chifotides and K. R. Dunbar, *Acc. Chem. Res.*, 2005, **38**, 146.
6 (*a*) A. Sreedhara and J. A. Cowan, *JBIC, J. Biol. Inorg. Chem.*, 2001, **6**, 337; (*b*) J. Reedijk, *J. Inorg. Biochem.*, 2001, **86**, 89; (*c*) S. E. Wolkenberg and D. L. Boger, *Chem. Rev.*, 2002, **102**, 2477.
7 (*a*) N. J. Farrer and P. J. Sadler, *Aust. J. Chem.*, 2008, **61**, 669; (*b*) P. C. A. Bruijnincx and P. J. Sadler, *Curr. Opin. Chem. Biol.*, 2008, **12**, 197.
8 (*a*) H. Y. Sang, J. L. Byoung, H. Kim and J. Suh, *J. Am. Chem. Soc.*, 2005, **127**, 9593; (*b*) S. A. Stoffregen, A. K. K. Griffin and N. M. Kostic, *Inorg. Chem.*, 2005, **44**, 8899; (*c*) V. Rajendiran, M. Palaniandavar, P. Swaminathan and L. Uma, *Inorg. Chem.*, 2007, **46**, 10446.
9 C. V. Kumar, A. Buranaprapuk, G. J. Opitech, M. B. Moyer, S. Jockusch and N. J. Turro, *Proc. Natl. Acad. Sci. U. S. A.*, 1998, **95**, 10361.
10 J. J. Thomas, R. Bakhtiar and G. Siuzdak, *Acc. Chem. Res.*, 2000, **33**, 179.
11 R. Bonnett, *Chemical Aspects of Photodynamic Therapy*, Gordon & Breach, London, UK, 2000.
12 M. R. Detty, S. L. Gibson and S. J. Wagner, *J. Med. Chem.*, 2004, **47**, 3897.
13 M. C. De Rosa and R. J. Crutchley, *Coord. Chem. Rev.*, 2002, **233–234**, 351.
14 B. W. Henderson, T. M. Busch, L. A. Vaughan, N. P. Frawley, D. Babich, T. A. Sosa, J. D. Zollo, A. S. Dee, M. T. Cooper, D. A. Bellnier, W. R. Greco and A. R. Oseroff, *Cancer Res.*, 2000, **60**, 525.
15 W.-H. Wei, Z. Wang, T. Mizuno, C. Cortez, L. Fu, M. Sirisawad, L. Naumovski, D. Magda and J. L. Sessler, *Dalton Trans.*, 2006, 1934.
16 M. Ochsner, *J. Photochem. Photobiol., B*, 1996, **32**, 3.
17 C. M. Allen, W. M. Sharman and J. E. van Lier, *Tumor Targeting Cancer Ther.*, 2002, 329.
18 (*a*) D. Ramaiah, I. Eckert, K. T. Arun, L. Weidenfeller and B. Epe, *Photochem. Photobiol.*, 2004, **79**, 99; (*b*) M. Kar and A. Basak, *Chem. Rev.*, 2007, **107**, 2861.
19 S. Atilgan, Z. Ekmekci, A. L. Dogan, D. Guc and E. U. Akkaya, *Chem. Commun.*, 2006, 4398.
20 F. S. Mackay, J. A. Woods, P. Heringová, J. Kašpárková, A. M. Pizarro, S. Parsons, V. Brabec and P. J. Sadler, *Proc. Natl. Acad. Sci. U. S. A.*, 2007, **104**, 20743.
21 (*a*) A. M. Angeles-Boza, H. T. Chifotides, J. D. Aguirre, A. Chouai, P. K.-L. Fu, K. R. Dunbar and C. Turro, *J. Med. Chem.*, 2006, **49**, 6841; (*b*) A. M. Angeles-Boza, P. M. Bradley, P. K.-L. Fu, S. E. Wicke, J. Bacsa, K. R. Dunbar and C. Turro, *Inorg. Chem.*, 2004, **43**, 8510; (*c*) D. A. Lutterman, P. K. L. Fu and C. Turro, *J. Am. Chem. Soc.*, 2006, **128**, 738.
22 M. Brindell, E. Kuliś, S. K. C. Elmroth, K. Urbańska and G. Stochel, *J. Med. Chem.*, 2005, **48**, 7298.
23 W. X. Belliston-Bittner, A. R. Dunn, Y. H. L. Nguyen, D. J. Stuehr, J. R. Winkler and H. B. Gray, *J. Am. Chem. Soc.*, 2005, **127**, 15907.
24 (*a*) A. M. Funston, C. Cullinane, K. P. Ghiggino, W. D. McFadyen, S. S. Stylli and P. A. Tregloan, *Aust. J. Chem.*, 2005, **58**, 206; (*b*) I. J. Bigio and S. G. Bown, *Cancer Biol. Ther.*, 2004, **3**, 259.
25 M. J. Rose, N. L. Fry, R. Marlow, L. Hinck and P. K. Mascharak, *J. Am. Chem. Soc.*, 2008, **130**, 8834.
26 S. Dhar, D. Senapati, P. K. Das, P. Chattopadhyay, M. Nethaji and A. R. Chakravarty, *J. Am. Chem. Soc.*, 2003, **125**, 12118.
27 A. K. Patra, S. Dhar, M. Nethaji and A. R. Chakravarty, *Chem. Commun.*, 2003, 1562.
28 S. Dhar, D. Senapati, P. A. N. Reddy, P. K. Das and A. R. Chakravarty, *Chem. Commun.*, 2003, 2452.
29 P. K. Sasmal, A. K. Patra, M. Nethaji and A. R. Chakravarty, *Inorg. Chem.*, 2007, **46**, 11112.
30 (*a*) M. Roy, B. Pathak, A. K. Patra, E. D. Jemmis, M. Nethaji and A. R. Chakravarty, *Inorg. Chem.*, 2007, **46**, 11122; (*b*) M. Roy, R. Santhanagopal and A. R. Chakravarty, *Dalton Trans.*, 2009, 1024.
31 M. Roy, S. Saha, A. K. Patra, M. Nethaji and A. R. Chakravarty, *Inorg. Chem.*, 2007, **46**, 4368.
32 S. Saha, R. Mazumdar, M. Roy, R. R. Dighe and A. R. Chakravarty, *Inorg. Chem.*, 2009, **48**, 2652.
33 M. Roy, T. Bhowmick, S. Ramakumar, M. Nethaji and A. R. Chakravarty, *Dalton Trans.*, 2008, 3542.
34 R. M. Burger, *Chem. Rev.*, 1998, **98**, 1153.
35 R. P. Hertzberg and P. B. Dervan, *J. Am. Chem. Soc.*, 1982, **104**, 313.
36 T. A. Van Den Berg, B. L. Feringa and G. Roelfes, *Chem. Commun.*, 2007, 180.
37 T. M. Rana and C. F. Meares, *J. Am. Chem. Soc.*, 1991, **113**, 1859.
38 T. M. Rana and C. F. Meares, *J. Am. Chem. Soc.*, 1990, **112**, 2457.
39 T. M. Rana and C. F. Meares, *Proc. Natl. Acad. Sci. U. S. A.*, 1991, **88**, 10578.
40 J. B. Ghaim, D. P. Greiner, C. F. Meares and R. B. Gennis, *Biochemistry*, 1995, **34**, 11311.
41 N. Ettner, G. A. Ellestad and W. Hillen, *J. Am. Chem. Soc.*, 1993, **115**, 2546.
42 N. Ettner, J. W. Metzger, T. Lederer, J. D. Hulmes, C. Kisker, W. Hinrichs, G. Ellestad and W. Hillen, *Biochemistry*, 1995, **34**, 22.
43 R. Miyake, J. T. Owens, D. Xu, W. M. Jackson and C. F. Meares, *J. Am. Chem. Soc.*, 1999, **121**, 7453.
44 G. Plourde, II, A. El-Shafey, F. S. Fouad, A. S. Purohit and G. B. Jones, *Bioorg. Med. Chem. Lett.*, 2002, **12**, 2985.
45 F. S. Fouad, J. M. Wright, G. Plourde, II, A. D. Purohit, J. K. Wyatt, A. El-Shafey, G. Hynd, C. F. Crasto, Y. Lin and G. B. Jones, *J. Org. Chem.*, 2005, **70**, 9789.
46 A. Suzuki, M. Hasegawa, M. Ishii, S. Matsumura and K. Toshima, *Bioorg. Med. Chem. Lett.*, 2005, **15**, 4624.
47 S. Tanimoto, S. Matsumura and K. Toshima, *Chem. Commun.*, 2008, 3678.
48 C. V. Kumar and A. Buranaprapuk, *Angew. Chem., Int. Ed. Engl.*, 1997, **36**, 2085.
49 C. V. Kumar and J. Thota, *Inorg. Chem.*, 2005, **44**, 825.
50 J. Thota, K. Bandara and C. V. Kumar, *Photochem. Photobiol. Sci.*, 2008, **7**, 1531 and references therein.
51 (*a*) A. Bergamo and G. Sava, *Dalton Trans.*, 2007, 1267; (*b*) P. J. Dyson and G. Sava, *Dalton Trans.*, 2006, 1929.

52 H.-K. Liu, S. J. Berners-Price, F. Wang, J. A. Parkinson, J. Xu, J. Bella and P. J. Sadler, *Angew. Chem., Int. Ed.*, 2006, **45**, 8153.
53 S. Pacor, S. Zorzet, M. Cocchietto, M. Bacac, M. Vadori, C. Turrin, B. Gava, A. Castellarin and G. Sava, *J. Pharmacol. Exp. Ther.*, 2004, **310**, 737.
54 G. Sava, I. Capozzi, K. Clerici, R. Gagliardi, E. Alessio and G. Mestroni, *Clin. Exp. Metastasis*, 1998, **16**, 371.
55 D. D. Perrin, W. L. F. Armarego and D. R. Perrin, *Purification of Laboratory Chemicals*, Pergamon Press, Oxford, U. K. 1980.
56 J. G. Collins, A. D. Sleeman, J. R. Aldrich-Wright, I. Greguric and T. W. Hambley, *Inorg. Chem.*, 1998, **37**, 3133.
57 R. L. Dutta and A. Syamal, *Elements of Magnetochemistry*, Affiliated East-West Press, New Delhi, 2nd edn, 1993.
58 C. J. O'Connor, *Prog. Inorg. Chem.*, 1982, **29**, 203.
59 G. M. Sheldrick, *SADABS, Version 2. Multi-Scan Absorption Correction Program*, Universität Göttingen, Göttingen, Germany, 2001.
60 G. M. Sheldrick, SHELX-97, *Programs for Crystal Structure Solution and Refinement*, Universität Göttingen, Göttingen, Germany, 1997.
61 C. K. Johnson, *ORTEP, III Report ORNL-5138*Oak Ridge National Laboratory, Oak Ridge, TN.
62 M. E. Reichmann, S. A. Rice, C. A. Thomas and P. Doty, *J. Am. Chem. Soc.*, 1954, **76**, 3047.
63 J. D. McGhee and P. H. von Hippel, *J. Mol. Biol.*, 1974, **86**, 469.
64 M. T. Carter, M. Rodriguez and A. J. Bard, *J. Am. Chem. Soc.*, 1989, **111**, 8901.
65 (*a*) J.-B. LePecq and C. Paoletti, *J. Mol. Biol.*, 1967, **27**, 87; (*b*) S. Neidle, *Nat. Prod. Rep.*, 2001, **18**, 291.
66 V. G. Cohen and H. Eisenberg, *Biopolymers*, 1969, **8**, 45.
67 A. Rentmeister, G. Mayer, N. Kuhn and M. Famulok, *Biol. Chem.*, 2008, **389**, 127.
68 *Structure-based drug design with discovery studio, Accelrys, version 0406*, Accelrys Software Inc., San Diego, 2003.
69 M. J. Frisch, G. W. Trucks, H. B. Schlegel, G. E. Scuseria, M. A. Robb, J. R. Cheeseman, J. A. Montgomery, Jr., T. Vreven, K. N. Kudin, J. C. Burant, J. M. Millam, S. S. Iyengar, J. Tomasi, V. Barone, B. Mennucci, M. Cossi, G. Scalmani, N. Rega, G. A. Petersson, H. Nakatsuji, M. Hada, M. Ehara, K. Toyota, R. Fukuda, J. Hasegawa, M. Ishida, T. Nakajima, Y. Honda, O. Kitao, H. Nakai, M. Klene, X. Li, J. E. Knox, H. P. Hratchian, J. B. Cross, V. Bakken, C. Adamo, J. Jaramillo, R. Gomperts, R. E. Stratmann, O. Yazyev, A. J. Austin, R. Cammi, C. Pomelli, J. Ochterski, P. Y. Ayala, K. Morokuma, G. A. Voth, P. Salvador, J. J. Dannenberg, V. G. Zakrzewski, S. Dapprich, A. D. Daniels, M. C. Strain, O. Farkas, D. K. Malick, A. D. Rabuck, K. Raghavachari, J. B. Foresman, J. V. Ortiz, Q. Cui, A. G. Baboul, S. Clifford, J. Cioslowski, B. B. Stefanov, G. Liu, A. Liashenko, P. Piskorz, I. Komaromi, R. L. Martin, D. J. Fox, T. Keith, M. A. Al-Laham, C. Y. Peng, A. Nanayakkara, M. Challacombe, P. M. W. Gill, B. G. Johnson, W. Chen, M. W. Wong, C. Gonzalez and J. A. Pople, *GAUSSIAN 03 (Revision C.02)*, Gaussian, Inc., Wallingford, CT, 2004.
70 J. M. Rademaker-Lakhai, D. Van Den Bongard, D. Pluim, J. H. Beijnen and J. H. M. Schellens, *Clin. Cancer Res.*, 2004, **10**, 3717.
71 J. Bernadou, G. Pratviel, F. Bennis, M. Girardet and B. Meunier, *Biochemistry*, 1989, **28**, 7268.
72 C. V Kumar, A. Buranaprapuk, H. C. Sze, S. Jockusch and N. J. Turro, *Proc. Natl. Acad. Sci. U. S. A.*, 2002, **99**, 5810.
73 R. E. Norman, S. Yan, L. Que, Jr., G. Backes, J. Ling, J. S. Loehr, J. H. Zhang and C. J. O'Connor, *J. Am. Chem. Soc.*, 1990, **112**, 1554.
74 S. Ménage, J. M. Vincent, C. Lambeaux, G. Chottard, A. Grand and M. Fontecave, *Inorg. Chem.*, 1993, **32**, 4766.
75 Q. X. Wang, K. Jiao, W. Sun, F. F. Jian and X. Hu, *Eur. J. Inorg. Chem.*, 2006, 1838.
76 R. B. Nair, E. S. Teng, S. L. Kirkland and C. J. Murphy, *Inorg. Chem.*, 1998, **37**, 139.
77 C. Rajput, R. Rutkaite, L. Swanson, I. Haq and J. A. Thomas, *Chem.–Eur. J.*, 2006, **12**, 4611.
78 C. Metcalfe, I. Haq and J. A. Thomas, *Inorg. Chem.*, 2004, **43**, 317.
79 U. Koen, S. Jiri and V. M. Luc, *Eur. J. Biochem.*, 2002, **269**, 2868.
80 T. A. Van Den Berg, B. L. Feringa and G. Roelfes, *Chem. Commun.*, 2007, 180.
81 K. Toshima, R. Takano, T. Ozawa and S. Matsumura, *Chem. Commun.*, 2002, 212.
82 S. Xu, S. Zhang, S. Chen, M. Zhang and T. Shen, *Photochem. Photobiol. Sci.*, 2003, **2**, 871.
83 P. Hanson, J. R. L. Smith and V. A. Osborne, *J. Chem. Soc., Perkin Trans. 2*, 1998, 2653.
84 M. C. B. de Oliveira, M. Scarpellini, A. Neves, H. Terenzi, A. J. Bortoluzzi, B. Szpoganics, A. Greatti, A. S. Mangrich, E. M. de Souza, P. M. Fernandez and M. R. Soares, *Inorg. Chem.*, 2005, **44**, 921.

